PAPER

Check for updates

New biobased-zwitterionic ionic liquids: efficiency and biocompatibility for the development of sustainable biorefinery processes†

Gaël Huet,[a] Monica Araya-Farias,[b,c] Ranim Alayoubi,[b] Sylvain Laclef, [ID][a] Benjamin Bouvier, [ID][a] Isabelle Gosselin,[b] Christine Cézard,[a] Romain Roulard,[d] Matthieu Courty,[e] Caroline Hadad,[a] Eric Husson,[b] Catherine Sarazin[b] and Albert Nguyen Van Nhien [ID] *[a]

A new family of biobased-zwitterionic ionic liquids (ZILs) have been synthesized starting from the renewable resource L-histidine natural amino acid and varying the lengths of the alkyl chains. These ZIL derivatives were firstly studied for their biocompatibility with different microorganisms including bacteria, molds and yeast. The obtained MIC values indicated that all the microorganisms were 5 to 25 times more tolerant to ZIL derivatives than the robust 1-ethyl-3-methylimidazolium acetate [C$_2$mim][OAc] used as a reference. Modeling studies also revealed that the presence of the cation and the anion on the same skeleton together with the length of the N-alkyl chain would govern the biocompatibility of these neoteric solvents. Among the different synthesized ZILs, the N,N′-diethyl derivative has been demonstrated to be a suitable eco-alternative to the classically used [C$_2$mim][OAc] for efficient pretreatment of harwood sawdust leading to a significant improvement of enzymatic saccharification. In addition, with up to a 5% w/v concentration in the culture medium, ZILs did not induce deleterious effects on fermentative yeast growth nor ethanol production.

Introduction

Ionic Liquids (ILs) are generally defined as organic salts based on a substituted heterocyclic cation with an organic or inorganic anion that melts below 100 °C. In addition to their thermal stability and low vapour pressure, some of them can be considered as suitable solvents to solubilize the constitutive biopolymers of lignocellulosic biomass (LCB). The IL-pretreatment of LCB demonstrated great potential for improving the availability of the constitutive polymers and thus their respective conversion into platform molecules, high added value chemicals or biofuels.[1–3] In this way, hydrophilic imidazolium-based ILs such as 1-ethyl-3-methylimidazolium acetate [C$_2$mim][OAc] have recently emerged in the biorefinery area as an efficient alternative to other pretreatments prior to LCB transformation.[4–8] Although their ability to disrupt or fractionate LCB under mild conditions is admitted, their scale-up at the industrial scale is still constrained by a questionable safety context due to their eco-cytotoxicity[9] and limited compatibility with the biological tools (enzymes and cells) used in the biorefinery processes. Moreover, the imidazolium-based ILs are mainly synthesized from non-renewable feedstock. They can also affect the performances of both enzymatic hydrolysis and microbial fermentation steps during LCB bioconversion processes. Indeed, the residual [C$_2$mim][OAc] amount entrapped in pretreated LCB can induce deactivation of hemicellulolytic enzymes during the hydrolysis step.[10] Similarly, inhibition of yeast growth was observed from a [C$_2$mim][OAc] concentration of 0.5% (w/w) during the fermentation step.[11–13]

To minimize these deleterious effects, successive washing of pretreated LCB requiring a large amount of water can be implemented after the pretreatment step, but this remained quite often insufficient.

[a]Laboratoire de Glycochimie, des Antimicrobiens et des Agroressources, UMR CNRS 7378, Université de Picardie Jules Verne - UFR des Sciences, 33 rue Saint Leu, 80039 Amiens Cedex, France. E-mail: albert.nguyen-van-nhien@u-picardie.fr

[b]Unité de Génie Enzymatique et Cellulaire, UMR CNRS 7025, Université de Picardie Jules Verne - UFR des Sciences, 33 rue Saint Leu, 80039 Amiens Cedex, France

[c]Macromolecules and Microsystems in Biology and Medecine, Institut Curie – Centre de Recherche – UMR 168 Physico Chimie Curie, Institut Pierre Gilles de Gennes pour la Microfluidique (IPGG), 6, rue Jean Calvin, 75005 Paris, France

[d]Plateforme de Microscopie Electronique – Université de Picardie Jules Verne, HUB de l'Energie, 33 rue Saint Leu, 80039 Amiens Cedex, France

[e]Laboratoire de Réactivité et Chimie des Solides, UMR CNRS 7314, Université de Picardie Jules Verne, HUB de l'Energie, 33 rue Saint Leu, 80039 Amiens Cedex, France

†Electronic supplementary information (ESI) available. See DOI: 10.1039/d0gc01002b

More recently, Kuroda *et al.*[14] demonstrated that ZILs could be an interesting alternative to ILs, particularly for LCB pretreatment prior to enzymatic saccharification followed by microbial production of ethanol. Nevertheless, these derivatives are not synthesized from renewable resources. Until now, few imidazolium-ZIL derivatives have been synthesized and characterized.[15,16] The studies have been mainly conducted in the area of (organo)catalysis.[17,18] The few examples described only their ability to dissolve[19] or to hydrolyse cellulose.[20] A strategy including the pretreatment of LCB with H_2SO_4, addition of $[(SO_3)^4C_4C_1im]$ zwitterions for *in situ* synthesis of a $[(HSO_3)^4C_4C_1im]HSO_4$ ionic liquid, and hydrolysis under microwave activation has been reported.[21] However the biocompatibility of these sulfonate derivatives towards hemicellulolytic enzymes and microorganisms could be questionable with regard to the cysteine content in proteins.[22]
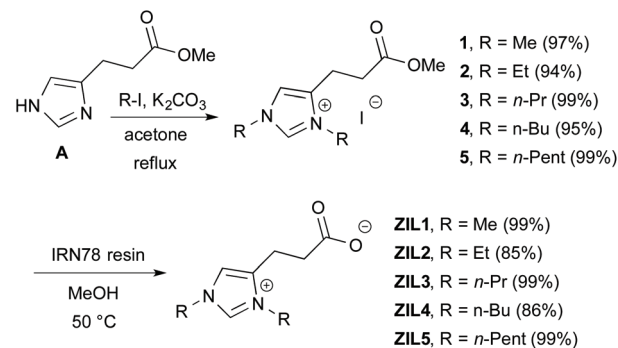
In the present work, we synthesized a new family of ZILs derived from the renewable natural amino acid L-histidine by varying the lengths of the alkyl chains. This new ZIL family was then described in terms of structural and physicochemical properties before interaction studies with membranes of microorganisms. This approach will give supplementary information for the development of lignocellulosic biorefinery. A cytotoxicity study of the ZILs was then carried out with representative micro-organisms: bacteria (unicellular and prokaryotic), yeasts (unicellular eukaryotic) and molds (pluricellular eukaryotic). A molecular modelling study was also undertaken to provide comprehensive information about ZILs and biological membrane interactions and explain the biocompatibility of ZILs with cells. The potential of ZILs for LCB pretreatment prior to enzymatic saccharification was then investigated and compared to the performances obtained with $[C_2mim][OAc]$. For this, two distinct representative LCB samples were selected: forest residues (oak sawdust) and dedicated crop (*Miscanthus × giganteus*). Finally, the biocompatibility of ZILs with the fermentative reference yeast, *S. cerevisiae*, was evaluated.

Results and discussion

Biobased-ZIL synthesis

ZIL derivatives have been synthesized following the general Scheme 1 starting from the known intermediate **A**, easily obtained in two steps from the commercially available biobased urocanic acid (resulting from enzymatic deamination of natural L-histidine amino acid).[23]

First, the iodide derivatives **1–5** were obtained by *N*-alkylation reaction, with yields ranging from 94% to 99%, by stirring 2.1 to 3 equivalents of the corresponding alkyl iodide with K_2CO_3 in acetone under reflux for 1 h to 3 days with the ester derivative **A**. In the presence of a strong basic resin such as Amberlite IRN78, **ZIL1** to **ZIL5** were obtained with yields ranging from 85% to 99%. In addition to these excellent yields, no chromatographic purification was necessary to obtain purified ZILs. A detailed experimental procedure is

Scheme 1 Biobased-ZIL synthesis.

reported in the ESI† together with the full characterization of each product.

Biobased-ZIL properties

Taking into consideration the melting point as one of the criteria for being considered as an IL, only **ZIL1** cannot be considered as an IL since its melting point is higher than 100 °C (+109 °C).

All the ZIL derivatives possessed a glass transition temperature (T_g) from −5 °C to −36 °C which increased in the opposite way to the length of the substituted alkyl chain, as already described by Biswas *et al.*[16] Data are summarized in Table 1 and compared to those of $[C_2mim][OAc]$, the IL mainly reported and used for the LCB pretreatment as a compromise between efficiency and toxicity.[24–26]

Thermogravimetric analysis (TGA) under an argon atmosphere (Fig. 1) of all ZIL derivatives was performed. The obtained thermograms showed a first mass loss at around 100 °C corresponding to the water content (values indicated in Table 1) reaching a value close to 16% for **ZIL1** showing the hygroscopic behavior of this compound. All biobased ZILs showed thermal stability limits of 250 °C to 315 °C, with little effect of the chain length in contradiction to the work reported by Dinda *et al.* in 2008.[27]

These values are very close to the temperature of degradation of 1-ethyl-3-methylimidazolium acetate $[C_2mim][OAc]$.

Table 1 Characterization data of the synthesized biobased-ZILs and commercially available $[C_2mim][OAc]$

Compound	$T_g{}^a$ (°C)	$T_m{}^a$ (°C)	DTG^b (°C)	Water content^b (%)
ZIL1	−5	+109	+255	15.8
ZIL2	−23	+97	+264	7.8
ZIL3	−30	—	+276	11.0
ZIL4	−35	+64	+280	9.5
ZIL5	−36	—	+314	5.9
$[C_2mim][OAc]$	—	—	+245	0.3

^{a} Determined using DSC under an argon atmosphere from 25 to −60 °C and then to 200 °C. ^{b} Determined using thermogravimetric analysis under an argon atmosphere from 50 to 800 °C.
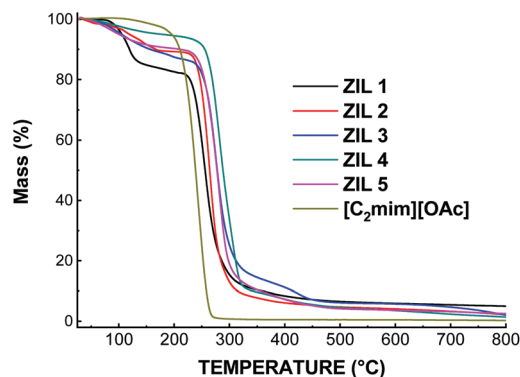
Fig. 1 TGA of synthesized biobased-ZILs and commercially available [C₂mim][OAc] under an argon atmosphere from 50 to 800 °C.

Biobased-ZIL cytotoxicity

In order to test the toxicity of the ZIL derivatives, we investigated the minimum inhibitory concentration (MIC) of the five ZILs on several microorganism species: (i) two bacteria, the Gram-negative *Escherichia coli* and the Gram-positive *Staphylococcus aureus*, (ii) two yeasts, the model ethanologenic *Saccharomyces cerevisiae* and the pentose-fermenting *Scheffersomyces stipitis* (formerly *Pichia stipitis*), and (iii) two common molds, *Aspergillus brasiliensis* (formerly *Aspergillus niger*) and *Penicillium chrysogenum* (Table 2). The versatile [C₂mim][OAc] IL was taken as a reference.[8]

Firstly, the five ZIL derivatives induced different MIC values depending on the lengths of the alkyl chains. The most biocompatible ZIL was **ZIL2** (ethyl chain) which showed the highest MIC values with all the strains tested, from 200 to 400 μg mL⁻¹ depending on the microorganisms: molds were the most tolerant to **ZIL2** (MIC: 300–400 μg mL⁻¹) compared to bacteria and yeasts (MIC 200–250 μg mL⁻¹). **ZIL1** exhibited a biocompatibility very close to **ZIL2** and the MIC values were identical for both molecules for *E. coli*, *S. aureus* and *S. cerevisiae*; they were slightly lower for *S. stipitis*, *A. brasiliensis* and *P. chrysogenum*. On increasing the ZIL chain length (**ZIL3** to **ZIL5**), MIC values decreased gradually indicating a greater toxicity. Bacteria, yeasts and molds were equally sensitive to **ZIL5** with a MIC value equal to 50 μg mL⁻¹ for all the microorganisms except for *P. chrysogenum* which showed a MIC of 100 μg mL⁻¹.

Secondly, the ZIL biocompatibility was much higher than that of the classical [C₂mim][OAc] IL for all the ZIL derivatives on all the microorganisms tested. For example on *S. cerevisiae*, the MIC values were 20 μg mL⁻¹ for [C₂mim][OAc], 250 μg mL⁻¹ for **ZIL2** and 50 μg mL⁻¹ for **ZIL5**. The only exception observed was specifically for **ZIL5** on *A. brasiliensis* which showed a MIC value of 50 μg mL⁻¹, whereas [C₂mim][OAc] induced a MIC of 150 μg mL⁻¹. Except for this particular condition, all ZIL derivatives were much more biocompatible than [C₂mim][OAc] until 25 times more for **ZIL2** on *S. aureus*.

Computational study

ILs are frequently described as perturbators of the cytoplasmic membrane integrity in microorganisms, inducing toxicity problems.[28–31]
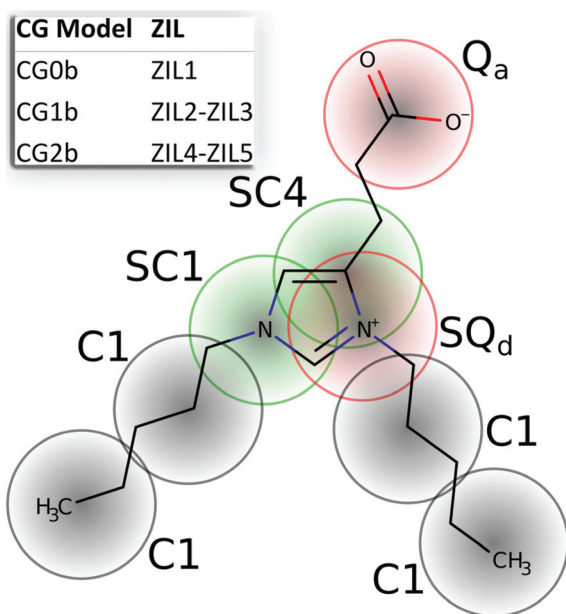
We thus used molecular simulations to study the membranotropic effects of ZILs of different alkyl chain lengths, compared to the [C₂mim][OAc] IL. We simulated the behavior of a typical *Saccharomyces cerevisiae* membrane under the influence of these ionic liquids at long timescales (4.5 μs) using the MARTINI coarse-grained (CG) force field,[32] whose performance for the simulation of membranes has been amply demonstrated (Marrink and Tieleman 2013). Inspired by the MARTINI representations of histidine, glutamic acid and linear alkyl chains, we designed three CG ZIL models, termed CG0b to CG2b, spanning atomistic **ZIL1** to **ZIL5**. Due to the degeneracy of the grain-to-atom mapping, each CG model represents more than one ZIL (Fig. 2). [C₂mim][OAc] was similarly constructed, on the basis of CG0b and CG1b but lacking the connection between beads SC4 and Qa. The models were validated by comparing structural and thermodynamic properties between matching atomistic and coarse-grained simulations.

The composition of the membrane, taken from the study by Vermaas *et al.*,[33] was chosen to mimic the experimental headgroup compositions of *S. cerevisiae* W303-1A, itself a good compromise between the compositions observed in the different *S. cerevisiae* strains. Each leaflet had a composition ratio of 30 : 14 : 12 : 9 : 4 : 1 of phosphatidyl choline (PC), phosphatidyl ethanolamine (PE), phosphatidyl inositol (PI), ergosterol, phosphatidyl serine (PS), and phosphatidic acid (PA) headgroups. The lipid tail composition and degree of unsaturations reproduced those observed by mass spectrometry and were comparable for all lipids involved: 55% palmitoyl–

Table 2 MIC values in μg mL⁻¹ on several microorganism species

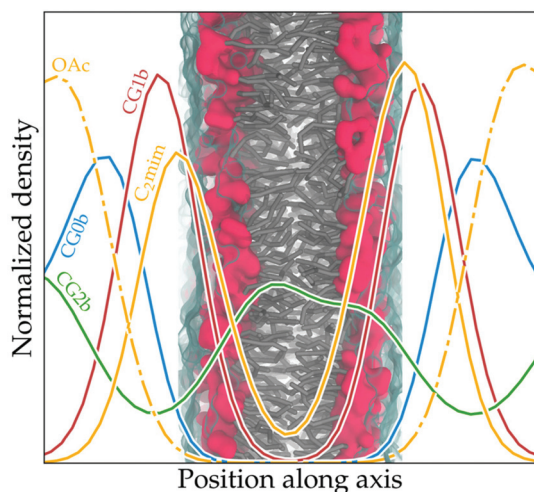| Compound	Bacteria		Yeasts		Molds	
	E. coli	*S. aureus*	*S. cerevisiae*	*S. stipitis*	*A. brasiliensis*	*P. chrysogenum*
ZIL1	200	250	250	150	200	350
ZIL2	200	250	250	200	300	400
ZIL3	150	100	200	150	300	350
ZIL4	50	50	100	50	150	250
ZIL5	50	50	50	50	50	100
[C₂mim][OAc]	10	10	20	20	150	90

Fig. 2 Left: Atom-to-bead mapping of the ZILs. The beads are labelled by their MARTINI atom type and colored according to their chemical character (red, green and black for charged, polar and apolar, respectively). Inset: Equivalence between CG and atomistic ZIL models. CG models are denoted as CGnb where *n* is the number of C1 beads of the alkyl chains.

ZIL1 (CG0b) had no effect: as can be seen from the position of the density peak, it tended to remain in solution and only formed transient contacts with the membrane. The density curve reveals that **ZIL2–ZIL3** (CG1b) also preserved the integrity of the membrane but interacted much more durably with it, at times penetrating the polar head group layer. The cation part of [C_2mim][OAc] showed a similar affinity for the membrane; despite slightly more frequent occurrences of ingress inside the head group layer, it preserved the membrane's overall integrity. However, in stark contrast to **ZIL2–ZIL3** where the cation and anion are covalently bound, the [OAc] anion became fully dissociated and remained in solution. Finally, **ZIL4–ZIL5** (CG2b) were seen to penetrate much deeper into the membrane, eventually splitting it into several components. The main steps of the membrane degradation mechanism are presented in Fig. 4. The ZIL molecules were seen to aggregate (upper left panel), forming a wedge which was driven between individual membrane components (lower panel); the local increase in lipid density which ensued destabilized the membrane *via* repulsions between the dipoles of the lipid headgroups. The effect was amplified by the dipolar nature of the ZILs themselves and their similarity to the membrane components, despite shorter hydrophobic tails. This resulted in the progressive separation of membrane patches (upper right panel) and the eventual breakup of the membrane in a simulation time of under 100 ns, which was roughly equivalent to
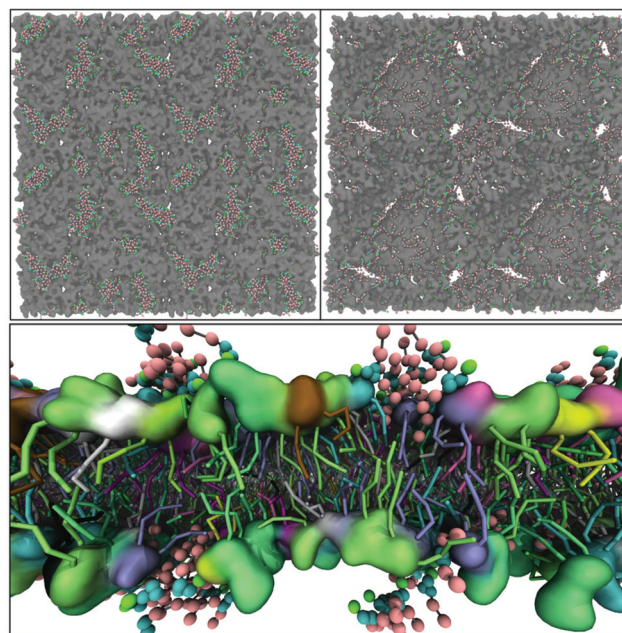
oleyl class (C16:0–18:1), 22% stearyl–linoleyl class (C18:0–C18:2), and 23% dioleyl class (C18:1–C18:1).

We first examined the durability of the contacts established between the different ionic liquids and the yeast membrane, and whether the latter's structural integrity was retained. The different CG IL and ZIL models were found to have strikingly different effects on the membrane (Fig. 3).

Fig. 3 Normalized density of ILs along the membrane normal axis. The position of the membrane is materialized (grey sticks: hydrophobic tails; red surface: polar heads; and blue surface: first hydration layer).

Fig. 4 Top: Initial events of yeast membrane breakup by the CG2b ZIL model, looking down on the membrane (gray surface). Snapshots at 10 ns into the simulation (top left), showing the clustering of the ZILs, and at 20 ns (top right), showing the onset of membrane splitting. Bottom: Insertion of ZIL alkyl chains between membrane components, seen from the side (lipids colored by type; surface = polar heads; and rods = hydrophobic tails). In all panels, ZIL beads are colored pink, blue and green for the alkyl, cyclic and acid parts, respectively.

0.5 μs considering the typical MARTINI kinetic speedup compared to all-atom models.[34]

The auto-aggregative power of **ZIL4–ZIL5** thus appeared crucial to their membranotropic properties. To confirm the importance of this effect, we simulated the solvated ZIL CG models in the absence of the membrane. At concentrations of 100 g L^{-1} in water, the ZIL models showed a propensity to form transient clusters which increased with the length of the alkyl chain. This can be clearly seen in Fig. 5, where the probability of finding another ZIL molecule in close contact to a given ZIL molecule is represented as isodensity surfaces. Indeed, at longer alkyl chain lengths (CG2b), the amphiphile and detergent-like character of ZILs becomes sufficient to trigger self-assembly, as observed in the case of lipids. The affinity of the ZILs for themselves thus appears to be the main driving force behind the breaking up of membranes by ZIL clusters. This corroborates experimental evidence that IL toxicity increases with the chain length due to membrane penetration.[28,29,35,36]

We then compared the effects of [C$_2$mim][OAc] and CG1b on the yeast membrane in more detail. As explained above, both exhibited similar affinities for the membrane and neither triggered a membrane breakup within the timescales under consideration. This is in agreement with several experimental studies which reported no significant effect on model membranes both for 1-ethyl-3-methylimidazolium chloride

[C$_2$mim][Cl] ILs with tails shorter than 6 carbon atoms[37] and for [C$_2$mim][OAc].[38] However, looking more closely at the time-resolved dynamics of the membranes in our simulations revealed striking differences between CG1b and [C$_2$mim][OAc]. [C$_2$mim][OAc] had a profound influence on the fundamental dynamical membrane properties such as the distribution of areas per lipid (APL, Fig. 6). In the presence of this IL, the distribution of APL over the membrane surface lost its homogeneity and featured locally large APL values, hinting at the formation of transient hole defects. Conversely, CG1b had no major impact on the distribution of APL. There is mounting evidence that such transient defects in membranes could affect biological function,[39] which could explain the higher toxicity of [C$_2$mim][OAc] compared to that of CG1b observed from the MIC results (Table 2). In particular, these defects could facilitate the penetration of water molecules into the membrane, which has well-known deleterious effects.[40] The benefits of substituting ILs by ZILs thus appear clearly in our simulation results, in good agreement with experimental evidence shown in Table 2. However, it should be kept in mind that owing to yeasts being complex microorganisms, the toxicity of ionic liquids can have many other causes apart from the destabilization of cell membranes which we simulate here. In particular, the complete dissociation of the [C$_2$mim][OAc] ion pair observed in our simulations increases the positive charge at the membrane surface and could disrupt the function of membrane transporters powered by transmembrane proton gradients. Some authors have also shown that ILs could interact with the cell wall polysaccharides in yeasts and modify the cell morphology.[11,13,41]

Other possible effects include modifications of the global cellular metabolism,[38] enhancement of ethanolic fermentation yields[11,13] or damage to yeast mitochondrial functions.[42] Some microorganisms also possess efflux pump systems for toxic products increasing the biocompatibility of ILs.[43] More research is needed to fully understand how (Z)ILs are tolerated by cells and some authors have even shown that the cytotoxicity of ILs is highly dependent on the biological system and that the same compound can be very toxic for an organism and without any effect for another.[44]
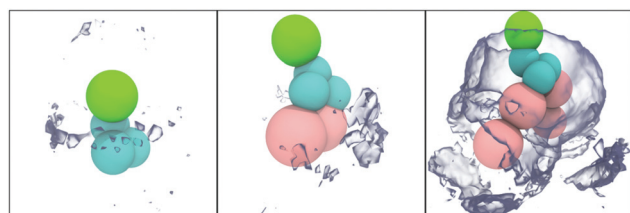
Fig. 5 70$^{\text{th}}$-percentile isodensity surfaces of ZIL molecules around a ZIL molecule (from left to right: CG0b, CG1b, and CG2b). ZIL beads are colored pink, blue and green for the alkyl, cyclic and acid parts, respectively.
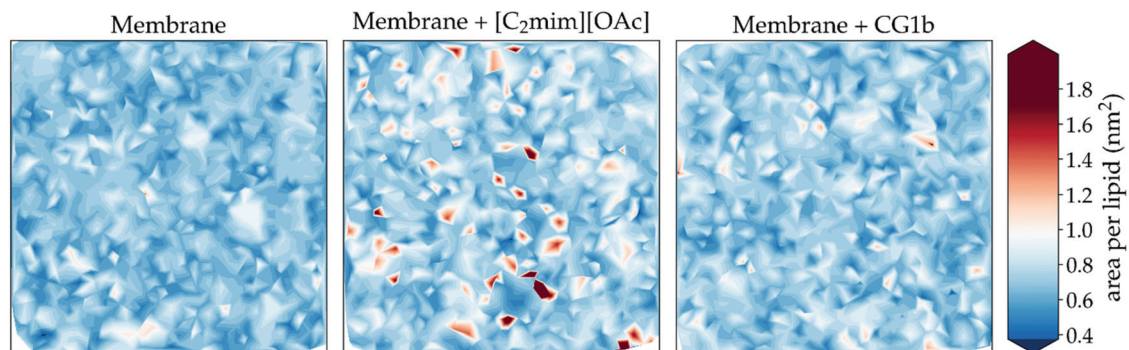
Fig. 6 Top view of the membrane surface, colored by area per lipid values, for representative conformations of the membrane in the absence of the IL (left), and in the presence of [C$_2$mim][OAc] (center) or CG1b (right).

ZIL pretreatment of lignocellulosic biomass: enzymatic saccharification and structural properties

Two main strategies are reported in the literature:

(i) the simultaneous strategy involving *in situ* enzymatic hydrolysis of LCB in diluted-IL aqueous media with an efficiency dependent on a compromise between a better accessibility (IL–biomass interactions) of the cellulosic fraction and enzyme deactivation (IL–cellulase interactions) and (ii) the sequential strategy defined as subsequent separated steps of IL-pretreatment of LCB and then enzymatic saccharification.[12,45,46]

However, the ILs classically used for these approaches exhibit some drawbacks in terms of toxicity, cost and recycling, thereby justifying the design of biosourced alternative non-conventional solvents.

Along these lines, the ability of carboxylate-type zwitterion ionic liquids to dissolve cellulose has been reported in the literature.[14] Among these new solvents, some would be suitable for improving enzymatic saccharification *via* a simultaneous strategy including an incubation of biomass in these solvents (8 h, 120 °C) before adding aqueous buffer and enzymes in one pot. In this context, we propose for the first time to investigate the potential of our newly synthesized ZILs to improve enzymatic saccharification through a sequential strategy. Two lignocellulosic biomass samples were rationally selected: *Miscanthus × giganteus* (monocot) as dedicated crops and oak (dicot) sawdust as forestry residues. These two biomass samples exhibited similar global chemical compositions in terms of cellulose and lignin contents.[5,6] Apart from these quantitative similarities, these two biomass samples are distinguished by their respective aromatic lignin content (hydroxyphenyl/guaiacyl/syringyl unit ratio) and hemicellulose composition[47,48] and can hence be considered as two distinct recalcitrant lignocellulosic matrices. Fig. 7 presents the glucose yields obtained after saccharification catalyzed by the cellulases of *T. reesei* before (untreated) and after a short pretreatment with the different ZILs at 110 °C.

Enzymatic saccharification of both untreated biomass samples led to similar yields of glucose in an average of 5.74 g/ 100 g of dried matter, confirming the recalcitrant properties of these two samples. Overall, ZIL pretreatments allowed the improvement of the performance of saccharification regardless of the biomass. The lengths of *N*-alkyl chains from the ZIL seem to have an influence on the ability of the ZIL to efficiently pretreat the biomass samples prior to their enzymatic saccharification. Indeed, the glucose yields increased with the increase of the *N*-alkyl chain length of the ZIL from 1 to 2 carbons and then decreased until 5 carbons. There is an obvious correlation between the alkyl chain length on ZIL derivatives and the performances of saccharification. Indeed, Singh *et al.* have recently shown that imidazolium cations with a lower alkyl chain length like [C_2mim][OAc] can interact with the aromatic rings of lignin moieties *via* π-stacking and H-bonding. In contrast, ILs with higher alkyl chain lengths cannot interact efficiently with the lignin due to steric hindrance and cause less biomass disorganization.

The solvation of lignocellulosic polymers by ZILs during the pretreatment step would thus be constrained by steric hindrance triggered by alkyl chains longer than 3 carbon atoms.

The improvement of saccharification appeared less marked for *Miscanthus × giganteus* than for oak sawdust with a maximal yield of glucose of 12.96% obtained after **ZIL2**-pretreatment *versus* 24.92% for oak sawdust (an increase by a factor of 4 in comparison with the untreated sample). These maximal performances obtained with **ZIL2** were then compared with those obtained after [C_2mim][OAc] pretreatment, the reference ionic liquid for biomass pretreatment reported in the literature.[49,50] Under our experimental conditions, [C_2mim][OAc] was shown to be more suitable than **ZIL2** to efficiently pretreat *Miscanthus × giganteus* prior to enzymatic saccharification with a glucose yield of 24.53 ± 0.76%. These results could be explained with SEM micrographs of *Miscanthus* before and after ZIL-pretreatment showing no significant disruption of the matrix, in contrast to [C_2mim][OAc]-pretreated sample (see ESI, Fig. S1†).

On the other hand, the pretreatment of oak sawdust with [C_2mim][OAc] led to efficient saccharification (glucose yield of 27.96 ± 1.98%), similar to that achieved after **ZIL2** pretreatment. Pretreatment by **ZIL2** would be thus a promising eco-alternative to [C_2mim][OAc] for oak sawdust pretreatment.

The structural changes induced by ZIL pretreatments were thoroughly studied in order to explain the improvement of saccharification after ZIL-pretreatment. The morphological properties of oak sawdust before and after ZIL-pretreatment were thus investigated by scanning electron microscopy (SEM) and compared to those induced by [C_2mim][OAc] pretreatment. Untreated oak sawdust (Fig. 8A) exhibited a complex organization with a highly fibrillar morphology of strongly agglomerated particles. After ZIL-pretreatment (Fig. 8C–G), the local organization of the lignocellulosic matrix was altered leading to more expanded materials with individualized fibers. These modifications suggested a better accessibility of the cellulosic fraction for enzymes according to the improvement of saccharification performances. Similar changes of the lignocellulosic
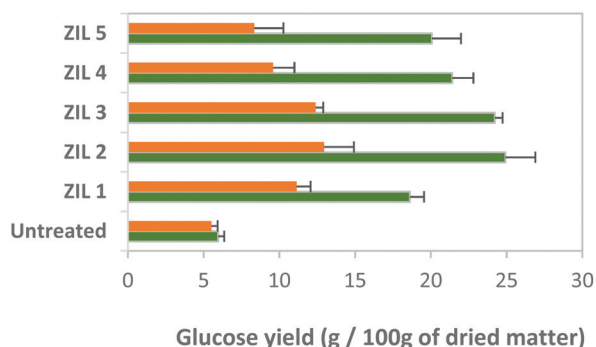

Fig. 7 Glucose yields (g per 100 g of dried matter) obtained after enzymatic saccharification of *Miscanthus × giganteus* (orange) and oak sawdust (green) before and after pretreatment with the different ZILs.
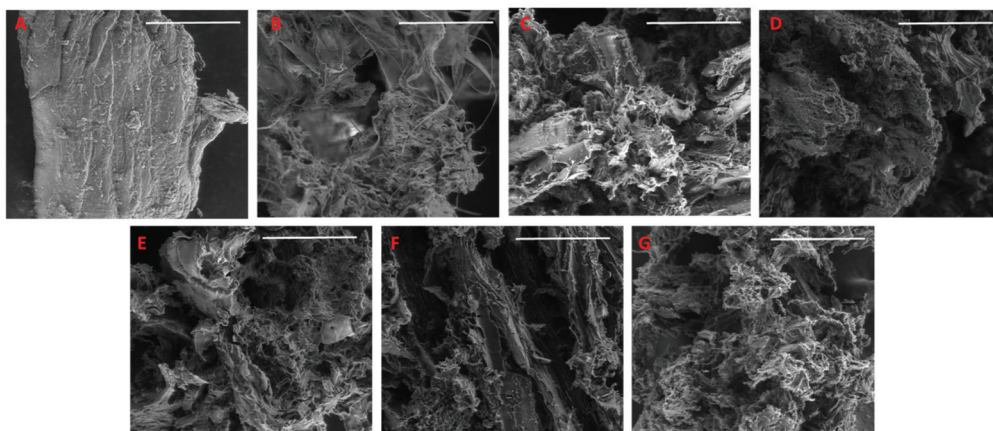
Fig. 8 SEM micrographs of untreated oak sawdust (A); [C$_2$mim][OAc]-pretreated oak sawdust (B); pretreated oak sawdust with **ZIL1** (C); **ZIL2** (D); **ZIL3** (E); **ZIL4** (F) and **ZIL5** (G); scale = 50 μm.

matrix were observed with [C$_2$mim][OAc] pretreatment (Fig. 8B) as previously reported in the literature.[6]

The impact on the structural properties of oak sawdust was also investigated by X-ray diffraction and thermogravimetric analyses before and after **ZIL2**-pretreatment and then compared to those obtained after [C$_2$mim][OAc] pretreatment.

The X-ray diffractogram of untreated sawdust showed a main broad peak at 22° (2θ) and two broad humps centered at ~16° (2θ) and 35° (2θ) (Fig. 9). This profile was characteristic of cellulose I which is a composite mixture of two distinct crystalline forms, cellulose Iα (triclinic) and cellulose Iβ (monoclinic) in agreement with literature data.[51] From these data, the crystallinity index of untreated sawdust was estimated at 51%.

In the case of **ZIL2**-pretreated sawdust, the crystallinity index was 46% and no shift was observed suggesting few effects of the ZIL on the supramolecular structure of the cellulosic fraction. Conversely, [C$_2$mim][OAc] pretreatment visibly modified the crystallographic structure of oak sawdust. Indeed, [C$_2$mim][OAc] pretreatment resulted in the broadening of the main peak, its shift to a lower angle (~20°) and the disappearance of the ~16° peak. The shift in the main peak to lower values of 2θ could indicate a transition from cellulose I

to cellulose II or an increase in the spacing between the stacked sheets of cellulose molecules. The decrease of the ~35° peak intensity could be due to the partial disruption of the microfibril alignment of the cellulose chains and/or a possible depolymerization. Finally, the crystallinity index decreased from 51 to 33%.

The TGA of the untreated- and pretreated-oak sawdust (Fig. 10) showed a first mass loss at around 100 °C corresponding to the evaporation of absorbed water molecules in the samples and, in agreement with the literature, the thermal decomposition of the sawdust between 200 and 400 °C.[52] Two pseudo-peaks, hemicellulose and cellulose, were present in the differential thermal analysis and their corresponding T_{max1} and T_{max2} are listed in Table 3. As demonstrated by Zhang *et al.*[53] the increase of the T_{max2} peak of the pretreated-oak sawdust with **ZIL2** is due to the removal of minerals which leads to an enhanced thermal stability. In the case of the [C$_2$mim][OAc]-pretreated oak sawdust sample, we observed a decrease of the T_{max2}. Indeed, XRD data showed the formation

Fig. 9 X-ray diffractogram of untreated oak sawdust (black), **ZIL2**-pretreated oak sawdust (red) and [C$_2$mim][OAc]-pretreated oak sawdust (blue) for 40 min at 110 °C.

Fig. 10 TGA analysis of untreated oak sawdust (black), **ZIL2**-pretreated oak sawdust (red) and [C$_2$mim][OAc]-pretreated oak sawdust (blue) for 40 min at 110 °C. Inset: De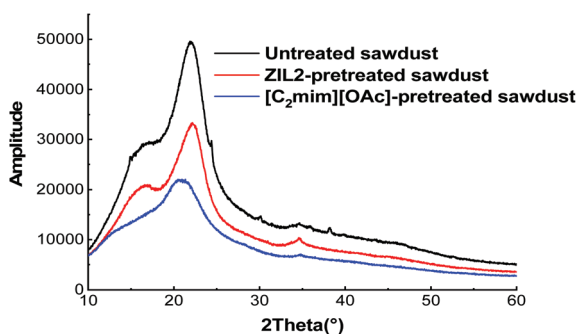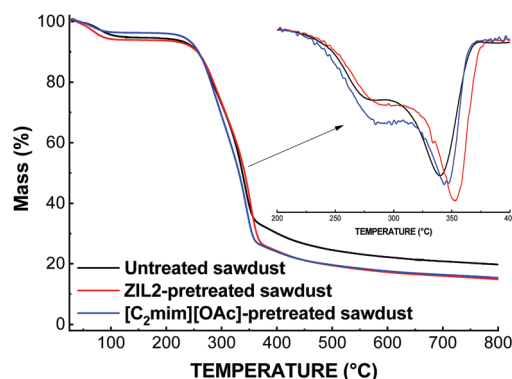rivatives of untreated oak sawdust (black), **ZIL2**-pretreated oak sawdust (red) and [C$_2$mim][OAc]-pretreated oak sawdust (blue) for 40 min at 110 °C.

Table 3 Positions of T_{max1} and T_{max2} peaks of untreated oak sawdust, ZIL2-pretreated oak sawdust and [C₂mim][OAc]-pretreated oak sawdust for 40 min at 110 °C

Compound	$T_{max1}{}^a$ (°C)	$T_{max2}{}^a$ (°C)	Water content[a]
Untreated oak sawdust	293	344	5.0%
ZIL2-pretreated oak sawdust	296	351	6.2%
[C₂mim][OAc] pretreated oak sawdust	281	339	3.8%

[a] Determined using thermogravimetric analysis under a nitrogen atmosphere from 50 to 800 °C.

of cellulose II which involved a severe degradation of the biomass components as already mentioned by Zhang *et al.*[53]
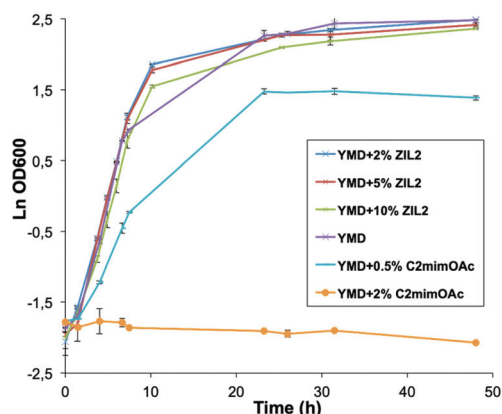
ZIL2-pretreatment would both preserve the supramolecular structure of cellulosic biomass and avoid undesirable partial depolymerization of cellulose while improving its accessibility to cellulases. **ZIL2** was thus demonstrated to be more suitable than [C₂mim][OAc] to implement eco-friendly pretreatment in preserving the structural integrity of the cellulosic polymer. We also suggested that the disruption mechanism of the ligno-cellulosic matrix induced by **ZIL2** would be thus distinct from that of [C₂mim][OAc].

Biocompatibility of ZILs at different concentrations for ethanol production

ZIL2 was the ZIL derivative giving better results of enzymatic hydrolysis after LCB pretreatment. We then searched if the potentially residual quantity of **ZIL2** remaining entrapped in the pretreated biomass could have a toxic effect on the downstream process such as yeast ethanolic fermentation or cellular production of any other compound of interest, as was observed with the classical [C₂mim][OAc] IL.[1–3] Indeed, we tried to determine if low **ZIL2** concentrations could influence the *S. cerevisiae* fermentation and ethanol production. For this purpose, we inoculated *S. cerevisiae* yeast cells in a YMD growth medium (glucose 20 g L⁻¹, yeast extract 3 g L⁻¹, malt extract 3 g L⁻¹ and peptone 3 g L⁻¹, pH = 4.8) eventually supplemented with different **ZIL2** or [C₂mim][OAc] concentrations. The growth was monitored by the measurement of the Optical Density at 600 nm (OD₆₀₀) (Fig. 11) and the quantification of ethanol produced by HPLC analysis (Table 4).

The results in Fig. 11 showed that the growth of *S. cerevisiae* was undisturbed by the presence of **ZIL2** up to a concentration of 10% (w/w) with exponential and stationary growth phases identical in terms of the duration and OD₆₀₀ values, whereas the reference [C₂mim][OAc] induced toxicity at a concentration as low as 0.5% (w/w) with a maximal OD₆₀₀ value 3 times lower than that in the YMD growth medium and no growth anymore at a concentration of 2% (w/w).

Ethanol production by *S. cerevisiae* was quantified by HPLC and the maximum ethanol yields are presented in Table 4. In these experiments, the only ethanologenic nutrient was the glucose present in the YMD medium.[11] The highest ethanol yield was obtained when *S. cerevisiae* was grown in the YMD

Fig. 11 Growth of *S. cerevisiae* in YMD medium supplemented with different concentrations of ZIL2 or [C₂mim][OAc].

Table 4 Maximum ethanol yields of *S. cerevisiae* grown under different culture conditions

Growth medium	Maximum ethanol yields (%)
YMD	84.2 ± 1.6
YMD + 2% **ZIL2**	83.7 ± 0.6
YMD + 5% **ZIL2**	80.9 ± 0.6
YMD + 10% **ZIL2**	69.1 ± 0.6
YMD + 0.5% [C₂mim][OAc]	81.5 ± 4.1
YMD + 2% [C₂mim][OAc]	N.D.

ND: No ethanol detected.

medium without any supplementation (84.2%). The addition of **ZIL2** at 2% had no effect on the ethanol production (83.7%), while at 5 and 10% a progressive decrease could be observed (80.9 and 69.1%, respectively). However, when [C₂mim][OAc] was added to the YMD medium, the ethanol yields drastically fell from 81.5% with 0.5% [C₂mim][OAc] down to zero with 2% IL.

Experimental

Chemicals, bacteria, yeasts, molds and enzymes

All the purchased materials were used without further purification. Mineral acids and bases were used in their highest concentrations commercially available, from Sigma-Aldrich (Steinheim, Germany). 1-Ethyl-3-methylimidazolium acetate ([C₂mim][OAc], >98%) was purchased from Solvionic SA (Verniolle, France). The microorganism strains used in this study were the bacteria *Escherichia coli* ATCC 10536 and *Staphylococcus aureus* subsp. *aureus* CIP 53.154, the yeasts *Saccharomyces cerevisiae* Type II from Sigma-Aldrich (Steinheim, Germany) and *Scherffersomyces stipitis* CLIB 187 (formerly *Pichia stipitis*) from the Institut Pasteur collection, and the molds *Aspergillus brasiliensis* ATCC 16404 (formerly *Aspergillus niger*) and *Penicillium chrysogenum* ATCC 10106. Bacteria were cultured at 37 °C in Luria Bertani (LB) broth

(peptone 10 g L⁻¹, yeast extract 5 g L⁻¹, and NaCl 5 g L⁻¹, pH 7.2), yeasts at 30 °C in Yeast-Malt-Dextrose (YMD) medium (glucose 20 g L⁻¹, yeast extract 3 g L⁻¹, malt extract 3 g L⁻¹, and peptone 3 g L⁻¹, pH 4.8) and molds at 25 °C in RPMI-1640 medium with L-glutamine and without sodium bicarbonate (from Sigma-Aldrich) in MOPS buffer (pH 7.0).

Cellulases from *Trichoderma reesei* were supplied by Sigma-Aldrich (Steinheim, Germany) and they present a specific activity of 5 IU mg⁻¹; one unit liberates 1.0 µmole of glucose from cellulose in one hour at pH 5.0 at 37 °C (2 h of incubation).

Miscanthus × giganteus was provided by UMR FARE (UMR 614 INRA URCA, Reims, France). Industrial sawdust of oak (*Quercus petraea*) was provided by the forest industry SARL Husson Paul (Bathelémont, Lorraine, France). Raw biomass samples were freeze-dried and then milled with a planetary ball mill (Retsch PM400) for 20 min at 300 rpm (particle sizes inferior to 255 µm).

Instruments

¹H and ¹³C nuclear magnetic resonance (NMR) spectra were recorded at 400 and 100 MHz using a Bruker DRX-400 spectrometer and at 300 and 75 MHz using a Bruker DRX-300 spectrometer. Chemical shifts are reported in parts per million relative to a residual solvent peak for CDCl₃ (¹H: δ = 7.26 ppm, ¹³C: δ = 77.16 ppm), DMSOd_6 (¹H: δ = 2.50 ppm, ¹³C: δ = 39.52 ppm) and MeODd_4 (¹H: δ = 3.31 ppm, ¹³C: δ = 49.00 ppm). The peak multiplicity is reported as: singlet (s), doublet (d), triplet (t), multiplet (m) and doublet of doublet (dd). High-resolution mass spectra (HRMS) were obtained by electrospray ionization (ESI) using a Micromass-Waters Q-TOF Ultima Global instrument. The morphology of untreated/pretreated biomass samples was investigated by scanning electron microscopy (SEM). The method consisted of observation in low vacuum mode (under partial vacuum pressure of water) without any sample preparation step. The microscope was an environmental high-resolution electron scanning microscope Quanta 200 FEG (FEI Co., USA) with a LF (Large Field) detector. The conditions of observation were as follows: acceleration voltage of 2 kV, work distance between 5 and 9 ppm and pressure between 0.5 and 2 mbar. Infrared spectra were obtained by using a Fourier-transform infrared (FT-IR) spectrometer (IRaffinity-1S, Shimadzu) and an ATR method with a germanium prism (MIRacle 10, Shimadzu). X-Ray Powder Diffraction (XRPD) patterns were acquired using a Bruker D4 Endeavor diffractometer equipped with a Cu anti-cathode (Kα radiation, operating at 40 kV–40 mA). Patterns were collected in a 2θ range of 10–60° with a step size of 0.03° and using a low background silicon holder (Bruker AXS, C79298A3244B261). The crystallinity index (CrI) was calculated from the XDR diffractograms using the amorphous subtraction region method. TGA was recorded on a Netzsch STA 449C Jupiter thermal analyser instrument equipped with a differential analysis microbalance coupled with a QMS 403 Aëolos mass spectrometer with a stainless steel capillary and a Secondary Electron Multiplier (SEV) detector (Channeltron).

The counting time for the mass spectrometer was 20 ms per (m/z) value (scanning width: m/z = 10–150 amu) with a resting time of 1 s. All the ionic derivatives were stored at room temperature in closed vials before analysis. The samples (approximately 20 mg of each compound) were heated in an alumina crucible under argon, by equilibrating at 25 °C, and following a ramp at 5 K min⁻¹ up to 800 °C and an isotherm under air atmosphere for 30 minutes (flow rate: 50 mL min⁻¹). Melting points were determined by differential scanning calorimetry on a DSC 204F1 supplied by NETZSCH-Gerätebau GmbH, Germany. All tests were performed at a heating rate of 10 K min⁻¹, between −60 and 200 °C under an argon atmosphere (50 mL min⁻¹) using about 10 mg of the sample. High performance liquid chromatography was performed with a Dionex Ultimate 3000 (Thermo Scientific, Sunnyvale, CA, USA) system consisting of an automatic sample changer, a pump and a detector type refractometer (RefractoMax 520), and the column was a HyperRez XP Carbohydrate H + (300 × 7.7 mm) equipped with a pre-column, kept at 75 °C. The isocratic mode is used, with ultra-pure water as the mobile phase; the flow rate was 0.6 ml min⁻¹. The retention time of glucose was 11.63 min and that of xylose was 13.81 min. Quantification was based on calibration curves established using standard glucose and xylose.

All molecular dynamics simulations and analyses thereof were performed using GROMACS.[54] All molecular graphics were generated using VMD.[55] All plots were designed with Matplotlib.[56]

Yeast fermentation

For the yeast growth experiments and the ethanolic fermentation of *S. cerevisiae*, cultures were realized in Erlenmeyer shake flasks in YMD medium eventually supplemented with ZIL2 at 2%, 5% or 10%, or [C₂mim][OAc] at 0.5% or 2% (all the percentages are w/w). The inoculum was a mid-log phase preculture. The yeast growth was followed by the measurement of the Optical Density at 600 nm (OD₆₀₀). The ethanol concentration was quantified by high performance liquid chromatography. The ethanol yields were calculated as:

$$Y_{\text{EtOH}} = (\text{concentration}_{\text{Ethanol}} \ (\text{g L}^{-1})/ \\ (\text{concentration}_{\text{Glucose}} \ (\text{g L}^{-1}) \times 0.511)) \times 100$$

where 0.511 represents the theoretical yield of ethanol from glucose.

Minimum inhibitory concentration (MIC) experiments

For the minimum inhibitory concentration (MIC) experiments, ZIL derivatives or [C₂mim][OAc] were dissolved at 450 µg mL⁻¹ in growth liquid media (LB for bacteria, YMD for yeasts and RPMI-1640 for molds), filter sterilized and serially diluted in sterile growth media. Each test tube was inoculated with cell suspensions (bacteria, yeasts or mold spores) with an OD₆₀₀ adjusted to 0.125 and incubated in a rotary shaker for 24 h for bacteria and yeasts or 72 h for molds under each optimal temperature condition. The cell growth was then measured

from the OD$_{600}$. The MIC was defined as the lowest concentration of the compound which prevented the visible growth of microorganisms,[57] *i.e.* that showed no increase in the OD$_{600}$. Each experiment was realized twice.

[C$_2$mim][OAc] and ZIL pretreatments

Lignocellulosic biomass (LCB) samples were subjected to pretreatments adapted from standard procedures reported in our previous studies.[5,6,48] LCB (2% w/v) was added to 1 mL of [C$_2$mim][OAc] or ZILs, and incubated in an oil bath at 110 °C with vigorous stirring for 40 min. After incubation, the LCB was precipitated by adding ultrapure water (2 : 1 v/v water/IL) to the mixture with vigorous stirring for 30 min in an ice bath to increase the polarity of the medium. The resulting suspension was subsequently centrifuged (10.1733g) (Allegra® 64R Beckman Coulter, Indianapolis, United States) at 20 °C for 20 min. This step was repeated 6 times until the amber-colored suspension became clear with conductivity lower than 200 µS cm^{-1}. This extensive washing step ensured minimization of residual [C$_2$mim][OAc] or ZILs to prevent potential deleterious effects on enzymatic hydrolysis.[8] The resulting insoluble substrate was then freeze-dried at room temperature for 24 h and collected for subsequent enzymatic hydrolysis.

Enzymatic saccharification

Cellulase-catalyzed hydrolysis were adapted from standard procedures described in our previous studies.[5,8,48] Freeze-dried untreated or pretreated LCBs were pre-incubated at 40 °C in 900 µL of acetate buffer (50 mM, pH 4.8) in Eppendorf tubes. After this pre-incubation step, reactions were started by adding cellulase mixtures from *T. reesei*. The final concentration of cellulase was 1 mg mL^{-1} (250 IU g^{-1} of substrate). The final volume of the reaction medium was 1 mL. Reactions were carried out at 40 °C and stirred at 1000 rpm (Eppendorf Thermomixer 5436). After 48 h, the reactions were stopped by incubation for 20 min at 90 °C to deactivate enzymes. Control experiments with buffer/substrate and with buffer/substrate/ thermally inactivated enzymes (90 °C, 20 min) were also performed.

Supernatants of hydrolysates were recovered by centrifugation (6000g, 15 min), diluted in ultra-pure water and filtered (0.2 µm) prior to HPAEC analyses. Each reaction was repeated 3 times. No sugar production was detected in the absence of native enzymes.

Glucose analysis

Glucose concentrations in the supernatants were determined by HPAEC using an analytical CarboPac PA-20 (150 × 3 mm) column equipped with a guard column (30 × 3 mm) (DIONEX, Thermo Fisher Scientific, Massachusetts, United States) and kept at 25 °C. Elution was carried out at a flow rate of 0.5 mL min^{-1} with a gradient method using sodium hydroxide and sodium acetate as the eluents, as described recently.[8] The injection volume was 10 µL. Quantification was based on the calibration curve using standard glucose solutions (0–0.1 g L^{-1}). The retention time of glucose was 11.50 min. The yields

of the substrate conversion into glucose were expressed as mean values with standard deviations (±) in g per 100 g of dry matter.

Synthesis of ZIL derivatives

General procedure for synthesis of iodide derivatives. To a solution of derivative **A** in acetone was added potassium carbonate (2 equivalents) and alkyl iodide (2.1 to 4 equivalents) and the mixture was stirred for 1 h to 3 days at 70 °C. After cooling at room temperature, the solvent was eliminated under vacuum and dichloromethane was added to the reaction mixture. After filtration and elimination of the solvent under vacuum, pure compounds **1–5** were obtained.

General procedure for saponification. To a solution of derivatives **1–5** in MeOH was added Amberlite IRN78 OH resin in a 1/6 ratio. The reaction was monitored by Mass Spectrometry (MS) with Electrospray Ionization (ESI). The reaction was stopped after total disappearance of the I$^-$ anion in the reaction media with MS (ESI) in negative mode. After stirring for 30 min at 40 °C, the solution was filtered and the solvent was eliminated under vacuum to afford pure **ZIL1–5**.

Computational study

Parameterization of the ZIL coarse-grained models. Atomic charges for the all-atom model of **ZIL4** were obtained using the RESP approach inside Antechamber.[58] Other forcefield parameters were gleaned from the GAFF forcefield.[59] **ZIL4** was placed in a cubic box (34 Å per side) and solvated with 798 TIP3P water molecules. The system was minimized to convergence, heated up to 300 K within 100 ps at a constant volume with the ZIL4 atoms restrained (500 kJ mol^{-1} nm^{-1}), and then for 100 ps at constant pressure. The restraints were progressively released over 1 ns. The velocity-rescaling thermostat time constant was raised from 0.2 ps^{-1} in the previous simulations to 2 ps^{-1}, and the Berendsen barostat (0.2 ps^{-1}) was switched to Parrinello–Rahman (10 ps^{-1}). The system was then simulated for a 50 ns production run. All simulations used periodic boundary conditions, particle-mesh Ewald electrostatics, and 1 nm Coulomb and van der Waals cutoffs. The time-dependent position of the atoms in the production simulation was used to obtain reference distributions of all possible bonds, angles and dihedral angles between the CG1b MARTINI beads. The parameters of the MARTINI model were adjusted so that the distributions obtained during a 50 ns coarse-grained simulation would match these reference distributions as closely as possible. This process yielded the CG1b model; the CG0b and CG2b models were generated by removing or adding a C1 MARTINI bead, with additional bond and angle parameters (in the case of CG2b) derived from the equivalent alkyl chain as already parameterized in MARTINI.

Coarse-grained system setup and simulation. The membrane was assembled from its individual lipid components, whose topologies are available in the MARTINI 2 forcefield,[33] using CHARMM-GUI.[60] It was subsequently energy-minimized to convergence. Several phases of constant temperature (velocity-rescaling thermostat, 300 K, 1.0 ps^{-1}) and pressure

(Berendsen barostat, 1 bar, 5.0 ps^{-1}) equilibration simulations with restrained lipid heads were successively performed: 500k, 200k, 100k, 50k and 50k steps of 2 fs, 5 fs, 10 fs, 15 fs and 20 fs, respectively, with restraints of 200, 100, 50, 20 and 10 kJ mol^{-1} nm^{-1}, respectively. The production simulations used a timestep of 20 fs, no restraints on any particle, and a Parrinello–Rahman barostat with a 12 ps^{-1} time constant. The ZILs were introduced into the equilibrated system by randomly replacing a number of water grains, performing 100 steps of steepest-descent minimization and 200k 10 fs steps of equilibration. The equilibrated simulation boxes had an approximate size of $20 \times 20 \times 8$ nm; their molecular compositions are given in the table presented in the ESI.† In all simulations, the membrane, ZIL and water used separate couplings to the heat bath; similarly, the membrane normal axis was coupled to the pressure bath independently from the other two axes. The electrostatic interactions employed a reaction-field scheme (cutoff: 1.1 nm, relative dielectric constant: 15) while the van der Waals interactions were computed using a potential-shift Verlet scheme (cutoff: 1.1 nm). The simulations of the ZILs solvated in water employed similar simulation parameters, but the equilibration phase was reduced to 500k steps of 10 fs without restraints.

Conclusions

The ZIL derivatives were obtained in a few steps with excellent overall yields without chromatography purification. These new biobased ZILs have shown very high biocompatibility towards several types of microorganisms: bacteria (unicellular prokaryotic cells), yeasts (eukaryotic unicellular cells) and molds (eukaryotic pluricellular cells), with **ZIL2** being the best tolerated by all the microorganisms. This was confirmed by our simulations as far as membranotropic effects in yeasts are concerned which showed that **ZIL2** preserved the cytoplasmic membrane integrity. Neither exchange nor dissociation can occur during the process due to the intrinsic ZIL structure, which could result in different toxicity-related mechanisms in the ZIL and imidazolium-IL derivatives. The fact that the cation and anion remain on the same skeleton would be thus an advantage compared to the classical imidazolium-IL as the zwitterionic nature of ZILs suppresses the hydrophobic interactions between the imidazolium *N*-alkyl chains and the phospholipids.[14]

Finally the biobased imidazolium-ZIL was demonstrated as an excellent eco-alternative to petroleum-based imidazolium ionic liquids for efficient pretreatment of hardwood prior to enzymatic saccharification.

The structural and morphological properties of ZIL-pretreated LCB suggested a different molecular mechanism during the pretreatment compared to that of [C$_2$mim][OAc]. ZIL-pretreatment preserved the supramolecular structure of the cellulosic fraction in LCB while increasing its accessibility and digestibility to enzymes. Moreover, a low ZIL concentration had no negative effect neither on *S. cerevisiae* growth

nor on ethanol production. Imidazolium based-ZILs are thus a promising alternative to ILs for the development of sustainable biorefinery processes.

Conflicts of interest

There are no conflicts to declare.

Acknowledgements

Notes and references

1 K. M. Docherty and J. C. F. Kulpa, *Green Chem.*, 2005, **7**, 185–189.
2 M. Ouellet, S. Datta, D. C. Dibble, P. R. Tamrakar, P. I. Benke, C. Li, S. Singh, K. L. Sale, P. D. Adams, J. D. Keasling, B. A. Simmons, B. M. Holmes and A. Mukhopadhyay, *Green Chem.*, 2011, **13**, 2743–2749.
3 I. R. Sitepu, S. Shi, B. A. Simmons, S. W. Singer, K. Boundy-Mills and C. W. Simmons, *FEMS Yeast Res.*, 2014, **14**, 1286–1294.
4 E. Husson, S. Buchoux, C. Avondo, D. Cailleu, K. Djellab, I. Gosselin, O. Wattraint and C. Sarazin, *Bioresour. Technol.*, 2010, **102**, 7335–7342.
5 T. Auxenfans, S. Buchoux, E. Husson and C. Sarazin, *Biomass Bioenergy*, 2014, **62**, 82–92.
6 T. Auxenfans, S. Buchoux, D. Larcher, G. Husson, E. Husson and C. Sarazin, *Energy Convers. Manage.*, 2014, **88**, 1094–1103.
7 E. Husson, C. Hadad, G. Huet, S. Laclef, D. Lesur, V. Lambertyn, A. Jamali, S. Gottis, C. Sarazin and A. Nguyen Van Nhien, *Green Chem.*, 2017, **19**, 4122–4131.
8 M. Araya-Farias, E. Husson, J. Saavedra-Torrico, D. Gérard, R. Roulard, I. Gosselin, H. Rakotoarivonina, V. Lambertyn, C. Rémond and C. Sarazin, *Front. Chem.*, 2019, **7**, 585–585.
9 A. Romero, A. Santos, J. Tojo and A. Rodríguez, *J. Hazard. Mater.*, 2008, **151**, 268–273.
10 T. Auxenfans, S. Buchoux, K. Djellab, C. Avondo, E. Husson and C. Sarazin, *Carbohydr. Polym.*, 2012, **90**, 805–813.
11 N. Mehmood, E. Husson, C. Jacquard, S. Wewetzer, J. Buchs, C. Sarazin and I. Gosselin, *Biotechnol. Biofuels*, 2015, **8**, 17.
12 T. Auxenfans, E. Husson and C. Sarazin, *Biochem. Eng. J.*, 2017, **117**, 77–86.
13 N. Mehmood, R. Alayoubi, E. Husson, C. Jacquard, J. Büchs, C. Sarazin and I. Gosselin, *Int. J. Mol. Sci.*, 2018, **19**, 887.

14 K. Kuroda, H. Satria, K. Miyamura, Y. Tsuge, K. Ninomiya and K. Takahashi, *J. Am. Chem. Soc.*, 2017, **139**, 16052–16055.

15 Z. Fei, D. Zhao, T. J. Geldbach, R. Scopelliti and P. J. Dyson, *Chem. – Eur. J.*, 2004, **10**, 4886–4893.

16 Y. Biswas, P. Ghosh and T. K. Mandal, *Chem. – Eur. J.*, 2018, **24**, 13322–13335.

17 A. Ferry, K. Schaepe, P. Tegeder, C. Richter, K. M. Chepiga, B. J. Ravoo and F. Glorius, *ACS Catal.*, 2015, **5**, 5414–5420.

18 S. Mahato, R. Chatterjee, N. C. Ghosal and A. Majee, *Synth. Commun.*, 2017, **47**, 1905–1915.

19 I. Grøssereid, K. C. Lethesh, V. Venkatraman and A. Fiksdahl, *J. Mol. Liq.*, 2019, **292**, 111353.

20 S. Suzuki, Y. Takeoka, M. Rikukawa and M. Yoshizawa-Fujita, *RSC Adv.*, 2018, **8**, 14623–14632.

21 H. Satria, K. Kuroda, T. Endo, K. Takada, K. Ninomiya and K. Takahashi, *ACS Sustainable Chem. Eng.*, 2017, **5**, 708–713.

22 S. Khademi, D. Zhang, S. M. Swanson, A. Wartenberg, K. Witte and E. F. Meyer, *Acta Crystallogr., Sect. D: Biol. Crystallogr.*, 2002, **58**, 660–667.

23 R. K. Dubey, N. Kumar and R. Jain, *Synth. Commun.*, 2012, **42**, 2207–2216.

24 D. Fu and G. Mazza, *Bioresour. Technol.*, 2011, **102**, 8003–8010.

25 N. Sun, H. Rodríguez, M. Rahman and R. D. Rogers, *Chem. Commun.*, 2011, **47**, 1405–1421.

26 S. K. Karatzos, L. A. Edye and W. O. S. Doherty, *Biotechnol. Biofuels*, 2012, **5**, 62–62.

27 E. Dinda, S. Si, A. Kotal and T. K. Mandal, *Chem. – Eur. J.*, 2008, **14**, 5528–5537.

28 S. P. Ventura, C. S. Marques, A. A. Rosatella, C. A. Afonso, F. Gonçalves and J. A. Coutinho, *Ecotoxicol. Environ. Saf.*, 2012, **76**, 162–168.

29 A. G. Santos, B. D. Ribeiro, D. S. Alviano and M. A. Z. Coelho, *RSC Adv.*, 2014, **4**, 37157–37163.

30 B. Jing, N. Lan, J. Qiu and Y. Zhu, *J. Phys. Chem. B*, 2016, **120**, 2781–2789.

31 K. Cook, K. Tarnawsky, A. J. Swinton, D. D. Yang, A. S. Senetra, G. A. Caputo, B. R. Carone and T. D. Vaden, *Biomolecules*, 2019, **9**, 251.

32 D. H. De Jong, G. Singh, W. F. D. Bennett, C. Arnarez, T. A. Wassenaar, L. V. Schäfer, X. Periole, D. P. Tieleman and S. J. Marrink, *J. Chem. Theory Comput.*, 2013, **9**, 687–697.

33 J. V. Vermaas, G. T. Beckham and M. F. Crowley, *J. Phys. Chem. B*, 2017, **121**, 11311–11324.

34 S. J. Marrink and D. P. Tieleman, *Chem. Soc. Rev.*, 2013, **42**, 6801–6822.

35 T. P. T. Pham, C.-W. Cho and Y.-S. Yun, *Water Res.*, 2010, **44**, 352–372.

36 G. Quijano, A. Couvert, A. Amrane, G. Darracq, C. Couriol, P. Le Cloirec, L. Paquin and D. Carrie, *Chem. Eng. J.*, 2011, **174**, 27–32.

37 C. M. N. Mendonça, D. T. Balogh, S. C. Barbosa, T. E. Sintra, S. P. M. Ventura, L. F. G. Martins, P. Morgado, E. J. M. Filipe, J. A. P. Coutinho, O. N. Oliveira and A. Barros-Timmons, *Phys. Chem. Chem. Phys.*, 2018, **20**, 29764–29777.

38 S.-K. Ruokonen, C. Sanwald, A. Robciuc, S. Hietala, A. H. Rantamäki, J. Witos, A. W. T. King, M. Lämmerhofer and S. K. Wiedmer, *Chem. – Eur. J.*, 2018, **24**, 2669–2680.

39 W. F. D. Bennett and D. P. Tieleman, *Acc. Chem. Res.*, 2014, **47**, 2244–2251.

40 R. Zappacosta, M. Semeraro, M. Baroncini, S. Silvi, M. Aschi, A. Credi and A. Fontana, *Small*, 2010, **6**, 952–959.

41 L.-P. Liu, M.-H. Zong, R. J. Linhardt, W.-Y. Lou, N. Li, C. Huang and H. Wu, *Biotechnol. Biofuels*, 2016, **9**, 266.

42 Q. Dickinson, S. Bottoms, L. Hinchman, S. McIlwain, S. Li, C. L. Myers, C. Boone, J. J. Coon, A. Hebert, T. K. Sato, R. Landick and J. S. Piotrowski, *Microb. Cell Fact.*, 2016, **15**, 17.

43 C. Yu, B. A. Simmons, S. W. Singer, M. P. Thelen and J. S. VanderGheynst, *Appl. Microbiol. Biotechnol.*, 2016, **100**, 10237–10249.

44 K. S. Egorova and V. P. Ananikov, *ChemSusChem*, 2014, **7**, 336–360.

45 S. Bose, D. W. Armstrong and J. W. Petrich, *J. Phys. Chem. B*, 2010, **114**, 8221–8227.

46 E. Husson, T. Auxenfans, M. Herbaut, M. Baralle, V. Lambertyn, H. Rakotoarivonina, C. Rémond and C. Sarazin, *Bioresour. Technol.*, 2018, **251**, 280–287.

47 J. S. Lupoi and E. A. Smith, *Appl. Spectrosc.*, 2012, **66**, 903–910.

48 J. Schäfer, M. Sattler, Y. Iqbal, I. Lewandowski and M. Bunzel, *GCB Bioenergy*, 2019, **11**, 191–205.

49 A. Brandt, J. Gräsvik, J. P. Hallett and T. Welton, *Green Chem.*, 2013, **15**, 550–583.

50 L. Liang, J. Yan, Q. He, T. Luong, T. R. Pray, B. A. Simmons and N. Sun, *Green Energy Environ.*, 2019, **4**, 432–438.

51 G. Cheng, P. Varanasi, C. Li, H. Liu, Y. Melnichenko, B. Simmons, M. Kent and S. Singh, *Biomacromolecules*, 2011, **12**, 933–941.

52 M. Guida and A. Hannioui, *J. Mater. Environ. Sci.*, 2019, **10**, 742–755.

53 J. Zhang, Y. Wang, L. Zhang, R. Zhang, G. Liu and G. Cheng, *Bioresour. Technol.*, 2014, **151**, 402–405.

54 M. J. Abraham, T. Murtola, R. Schulz, S. Páll, J. C. Smith, B. Hess and E. Lindahl, *SoftwareX*, 2015, **1–2**, 19–25.

55 W. Humphrey, A. Dalke and K. Schulten, *J. Mol. Graphics*, 1996, **14**, 33–38.

56 J. D. Hunter, *Comput. Sci. Eng.*, 2007, **9**, 90–95.

57 J. M. Andrews, *J. Antimicrob. Chemother.*, 2001, **48**, 5–16.

58 J. Wang, W. Wang, P. A. Kollman and D. A. Case, *J. Mol. Graphics Modell.*, 2006, **25**, 247–260.

59 J. Wang, R. M. Wolf, J. W. Caldwell, P. A. Kollman and D. A. Case, *J. Comput. Chem.*, 2004, **25**, 1157–1174.

60 S. Jo, T. Kim, V. G. Iyer and W. Im, *J. Comput. Chem.*, 2008, **29**, 1859–1865.